Organic Electronics 13 (2012) 856–863

Contents lists available at SciVerse ScienceDirect

Organic Electronics

journal homepage: www.elsevier.com/locate/orgel

Nanoporous platinum counter electrodes by glancing angle deposition for dye-sensitized solar cells

Sui-Ying Hsu [a], Chih-Hung Tsai [a,*], Chun-Yang Lu [a], Yu-Tang Tsai [a], Tsung-Wei Huang [a], Yuan-Hsuan Jhang [a], Yan-Fang Chen [a], Chung-Chih Wu [a,*], Yen-Shan Chen [b]

[a] Department of Electrical Engineering, Graduate Institute of Photonics and Optoelectronics, and Graduate Institute of Electronics Engineering, National Taiwan University, Taipei 10617, Taiwan, ROC
[b] AU Optronics Corporation, Hsinchu 30078, Taiwan, ROC

ARTICLE INFO

Article history:
Received 16 November 2011
Received in revised form 31 January 2012
Accepted 31 January 2012
Available online 19 February 2012

Keywords:
DSSCs
Counter electrode
Porous
Nanostructure
Platinum
GLAD

ABSTRACT

We report an effective way to produce nanoporous Pt counter electrodes of dye-sensitized solar cells by the glancing-angle deposition (GLAD) technique. By controlling the orientation of the substrate relative to the incident Pt vapor flux during the deposition, nanoporous films composed of inclined nm-scale columns were produced through the self-shadowing effect. Pt counter electrodes having varied nanoporous structures were characterized for their morphological and electrochemical properties, and were subjected to device studies to establish the correlation with DSSC characteristics/performances. The results suggest that the nanoporous GLAD Pt electrodes can effectively enhance active surface areas, the catalytic ability and charge exchange at the Pt/electrolyte interface of a DSSC. As a result, the quantum efficiency, short-circuit current, and power conversion efficiency of the DSSC can be enhanced by up to 12–13% with using the nanoporous GLAD Pt counter electrodes.

1. Introduction

Increasing energy demands and concerns about global warming have encouraged scientists to develop low-cost and easily accessible renewable energy sources in recent years [1–3]. Dye-sensitized solar cells (DSSCs) offer the advantages of relatively high efficiencies, simple device structures, cost-effective manufacturing, and variety and flexibility in applications, thus emerging as one of the most promising solar cell technologies [4–8].

A typical DSSC consists of a transparent conductive substrate, a porous thin-film photoelectrode composed of TiO_2 nanoparticles, dyes, an electrolyte, and a counter electrode [9]. The counter electrode, as one important component in DSSCs, is usually composed of a conductive catalytic layer. The role of the conductive catalytic layer as the counter electrode of the DSSC is to catalyze the reduction of the I_3^- ions in the electrolyte produced during the regeneration of the oxidized dyes (through the oxidation of iodide ions in the electrolyte). The requirements for the counter electrode in a DSSC are thus low charge-transfer resistance and high exchange current densities for effective reduction of the oxidized species, and good chemical/electrochemical stability in the electrolyte systems used in DSSCs [10]. Among various materials used for counter electrodes of DSSCs [11–15], platinum (Pt) is most effective due to its excellent electrocatalytic activity for reduction of triiodide. Researchers had thus been engaged in investigating different depositions of Pt counter electrodes and their influences on DSSC characteristics. For instance, researchers had studied effects of different Pt thicknesses and effects of various deposition techniques, such as physical vapor-phase deposition, electrodeposition, electrochemical deposition and thermal decomposition [16–19]. On the other hand, although producing nanoporous structures in Pt counter electrode to increase its surface area also appears

* Corresponding authors. Tel.: +886 2 33663636; fax: +886 2 33669404.
E-mail addresses: chihhtsai@ntu.edu.tw (C.-H. Tsai), chungwu@cc.ee.ntu.edu.tw (C.-C. Wu).

1566-1199/$ - see front matter © 2012 Elsevier B.V. All rights reserved.
doi:10.1016/j.orgel.2012.01.035

an effective way to enhance the catalytic capability of the counter electrode and thus the DSSC efficiency, yet not many systematic studies had been conducted.

In this work, we report an effective way to produce nanoporous structures in Pt counter electrodes of dye-sensitized solar cells by the glancing-angle deposition (GLAD) technique [20]. By controlling the orientation of the substrate relative to the incident Pt vapor flux during the Pt deposition, nanoporous films composed of inclined nm-scale columns were produced through the self-shadowing effect [21]. The GLAD Pt counter electrodes were characterized for their physical and electrochemical properties and were subjected to device studies. Results show that GLAD Pt counter electrodes can provide larger reactive surface areas between the Pt and the electrolyte and are beneficial to conversion efficiencies of DSSCs.

2. Experiments

2.1. Glancing-angle deposition (GLAD) of Pt counter electrodes

The GLAD technique [22] was used to deposit nanoporous Pt counter electrodes in this work. In traditional vacuum deposition of thin films, the stream of vapor-phase atoms strikes the substrate perpendicularly. Yet in GLAD deposition, as illustrated in Fig. 1(a), the substrate is tilted and thus the deposition flux is incident onto a substrate with a relatively large tilt angle (α) with respect to the surface normal. As initial atoms condense on the substrate, they agglomerate into microscopic clumps or nucleation sites. Line-of-sight shadowing prevents following atoms from condensing in the regions immediately behind the nucleus; thus, atoms can deposit only on the tops of nuclei (Fig. 1(b)). As the deposition continues, the nuclei develop into columnar structures that are oriented toward the vapor source [23]. Varying the substrate tilt angle α can in general control separation between columns and the porous structure (e.g., porosity) [24].

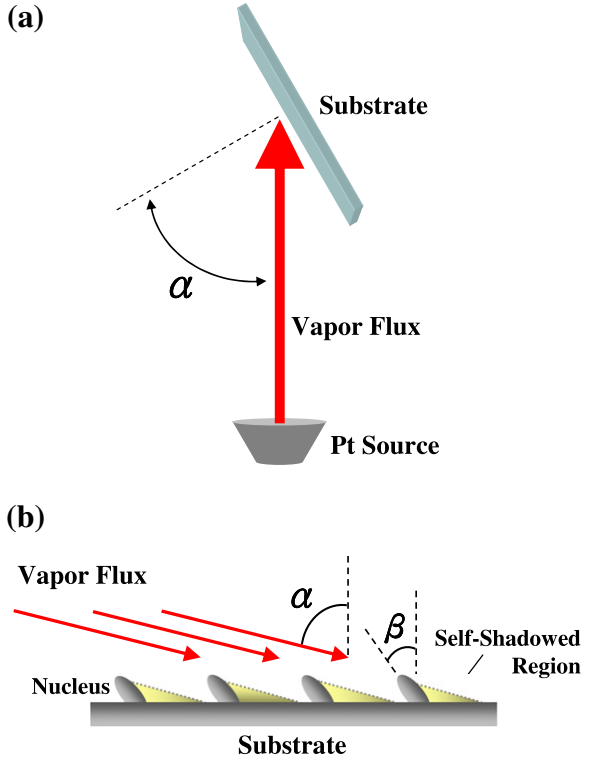

Fig. 1. (a) Schematic illustration of the GLAD technique, and (b) schematic illustration of the self-shadowing effect and formation of columnar (nanorod-like) structures in GLAD.

In this work, GLAD Pt films for counter electrodes of DSSCs were grown on flat glass substrates by electron-beam evaporation. The vacuum chamber used had a base pressure of about 2×10^{-6} Torr and the Pt deposition rate (referring to the surface normal direction) was kept at 0.5 Å/s, as monitored by a quartz-crystal thickness monitor. Prior to the deposition of GLAD Pt films with different substrate tilt angles (α), a 40-nm-thick Pt film was first deposited on the flat glasses with a 0° tilt angle (i.e., $\alpha = 0°$) to produce a dense and conducting Pt layer. On top of such dense Pt layers, the GLAD Pt films were then deposited with different substrate tilt angles, 0° for Pt electrode Pt0°(200), 70° for Pt electrode Pt70°(200), 75° for Pt electrode Pt75°(200) and 85° for Pt electrode Pt85°(200). The Pt electrode sample Pt0°(200) (deposited at $\alpha = 0°$) was indeed a dense Pt film obtained by the traditional normal-direction deposition and was used as a reference for comparison with other GLAD Pt electrodes. Due to the tilted deposition, the actual film thicknesses of GLAD films (t_{actual}) were in general different from the set film thicknesses (t_0) for normal-direction deposition. In this work, the t_0 in the second deposition step (i.e., after the first 40-nm-thick dense layer) was set at 200 nm and t_{actual} was characterized by the cross-section scanning electron microscopy (SEM). For a fair comparison, a GLAD Pt electrode Pt85°(300) (Pt deposited with a tilt angle of 85° and a set film thickness of 300 nm) with an actual layer thickness similar to that of Pt75°(200) was also prepared and characterized.

2.2. Characterization of GLAD Pt counter electrodes

Scanning electron microscopy (SEM) and atomic force microscopy (AFM) were used to characterize the morphology, surface topography and roughness of the GLAD Pt counter electrodes.

Electrochemical activities of the counter electrode for I_3^- reduction were examined by cyclic voltammetry (CV). The cyclic voltammetry was employed to characterize the relative catalytic ability/active surface areas of the GLAD Pt counter electrodes. The CV measurements were conducted using a three-electrode electrochemistry system (Gamry instrument). The Pt counter electrodes under testing were used as the working electrode, Pt foil as the counter electrode, and Ag/Ag^+ as the reference electrode [15]. The scan rate used was 100 mV/s, while the electrolyte was the acetonitrile solution containing 10 mM LiI, 1 mM I_2, and 100 mM $LiClO_4$.

2.3. DSSC Fabrication

Fig. 2 shows the schematic device structure of the DSSC using the GLAD Pt as the counter electrode. In fabrication

of devices, two types of fluorine-doped tin oxide (FTO) transparent conductors on glass substrates (FTO2% and FTO17%) having different textures and properties were used (purchased from the commercial source, Solaronix and Hartford Glass). Their properties are summarized in Table 1. The FTO glass substrate FTO2% had smaller textures (smaller FTO grain sizes), smaller surface roughness and lower optical haze (i.e., weak optical scattering capability), while FTO glass substrate FTO17% had larger textures (larger FTO grain sizes), larger surface roughness and higher optical haze (i.e., stronger optical scattering capability). Both FTO glass substrates had similar sheet resistance of 10–15 Ω/sq and similar total transmittance (T_{total}) of 80–85% as determined by a UV–Vis spectrophotometer equipped with an integrating sphere. In this work, the FTO glass substrate FTO2% with a smaller roughness and optical haze was first used to study the influences of various nanoporous GLAD Pt counter electrodes on DSSC characteristics. After determining the effects of different GLAD Pt electrodes, the FTO glass substrate FTO17% with a larger texture and optical haze was then applied in combination with the picked GLAD Pt electrode to further optimize the DSSC performances.

In fabrication of DSSC devices, the FTO glass substrates were first cleaned in a detergent solution using an ultrasonic bath and then were rinsed with water and ethanol. A layer of 20-nm-sized anatase TiO_2 nanoparticles was then coated on the FTO by the doctor-blade method. After drying the film at 120 °C, another layer of 400-nm-sized anatase TiO_2 nanoparticles was then coated as the light scattering layer. The resulting working electrode was composed of a 12-μm-thick transparent TiO_2 nanoparticle layer (average particle size: 20 nm) and a 4-μm-thick TiO_2 scattering layer (average particle size: 400 nm) [25]. The thickness of the TiO_2 nanoparticle layer had been optimized by balancing the tradeoff between optical absorption and the electrical transport properties. The nanoporous TiO_2 electrodes were then heated in an atmospheric oven first by gradually ramping the temperature from 150 °C to 500 °C and then at 500 °C for 30 min. After cooling, the nanoporous TiO_2 electrodes were immersed into a dye solution at room temperature for 24 h for dye adsorption. The dye solution was composed of 0.5 mM ruthenium dye N719, [cis-di(thiocyanato)-N-N′-bis(2,2′-bipyridyl-4-carboxylic acid-4′-tetrabutyl-ammonium carboxylate) ruthenium (II)] [26], and 0.5 mM chenodeoxycholic acid (CDCA, as a co-adsorbent) in the acetonitrile/tert-butanol mixture (1:1) [27].

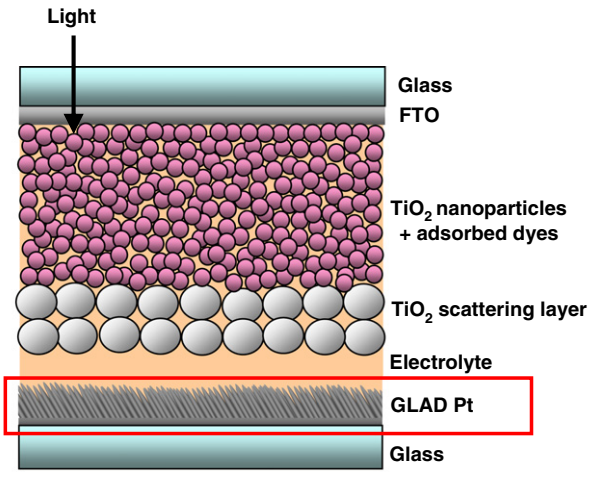

Fig. 2. The schematic device structure of the DSSC using the GLAD Pt as the counter electrode.

Various Pt counter electrodes for the DSSC were prepared as described in the Section 2.1. The dye-adsorbed TiO_2 working electrode and a counter electrode were then assembled into a sealed DSSC cell with a sealant spacer between the two electrode plates. A drop of electrolyte solution [0.6 M 1-butyl-3-methylimidazolium iodide (BMII), 0.03 M I_2, 0.5 M 4-tert-butylpyridine, and 0.1 M guanidinium thiocyanate in a mixture of acetonitrile-valeronitrile (85:15, v/v)] was injected into the cell through a drilled hole. Finally, the hole was sealed using the sealant and a cover glass.

2.4. DSSC characterization

The photocurrent–voltage (I–V) characteristics of the DSSCs were measured under illumination of the simulated AM1.5G solar light from a 300-W Xenon lamp solar simulator. The incident light intensity was calibrated as 100 mW/cm^2. Photocurrent–voltage curves were obtained by applying an external bias voltage to the cell and measuring the generated photocurrent. The current–voltage characteristics of DSSCs were used to extract the short-circuit current density (J_{SC}), open-circuit voltage (V_{OC}), fill factor (FF), and power conversion efficiency (Eff.) of the DSSCs [28,29]. The incident photon-to-current conversion efficiency (IPCE) spectra of the devices were measured by using a 75-W Xenon arc lamp as the light source coupled to a monochromator. The IPCE data were taken by illuminating monochromatic light on the solar cells (with the wavelength from 300 nm to 800 nm) and measuring the short-circuit current of the solar cells [30]. The IPCE measurement was conducted with a lock-in amplifier, a low-speed chopper, and a bias light source under the full computer control.

In addition to the standard I–V and IPCE characterization of solar cells, in this study, the electrochemical impedance spectroscopy (EIS) was also used to analyze the internal impedance properties of DSSCs [31,32]. The electrochemical impedance spectroscopy of the cells was measured by using an impedance analyzer with a frequency range of 20 Hz–1 MHz. In this study, during the impedance measurement, the cell was under the constant AM 1.5G 100 mW/cm^2 illumination. The impedance of the cell (throughout the frequency range of 20 Hz to 1 MHz) was then measured by applying a bias at the open-circuit voltage V_{OC} of the cell (namely, under the condition of no dc electric current) and by using an ac amplitude of 10 mV.

3. Results and discussions

3.1. Properties of GLAD Pt counter electrodes

Fig. 3 shows the cross-section and top-view SEM images of the GLAD Pt electrodes deposited at different substrate tilt angles α, with t_0 being all set around 200 nm. The

Table 1
Characteristics of different FTO substrates used in this work.

FTO substrate	FTO thickness (nm)	FTO grain size (nm)	Roughness (nm)	Sheet resistance (Ω/sq)	T_{total} (550 nm)	Haze (550 nm)
FTO2%	~400	~100–200	9.14	15	85%	2%
FTO17%	~800	~400 + ~100–200	38.42	10	80%	17%

characteristics of various Pt electrodes are also summarized in Table 2. Under the traditional normal-direction deposition ($\alpha = 0°$ case), a dense Pt film was obtained as revealed by both the cross-section and top-view SEM. The (vertical) film thickness of sample Pt0°(200), determined from the cross-section SEM was 206.2 nm, close to the set t_0 = 200 nm. When tilting the substrate during Pt deposition ($\alpha = 70°–85°$ cases), due to the self-shadowing effect of the GLAD, inclined columnar (nano-rod-like) structures were clearly observed in the cross-section SEM. The column tilt angle β (relative to the surface normal) in general increased with the substrate tilt angle α. From the cross-section SEM, β was estimated to be 42°, 47° and 56° for $\alpha = 70°$, 75° and 85°, respectively. The observed column tilt angle β was smaller than the substrate tilt angle α, a typical phenomenon in GLAD deposition [33]. Furthermore, with the tilted deposition, the actual film thickness t_{actual} significantly deviated from the t_0 (200 nm) and in general decreased with the substrate tilt angle α. For $\alpha = 70°$, 75° and 85°, t_{actual} was estimated to be 100.3 nm, 90.9 nm and 74.1 nm, respectively. From the top-view SEM, it was seen that when increasing the substrate tilt angle, the separation between inclined columns was enlarged (i.e., the column density decreased) and the porosity of the film increased (i.e., more porous). Fig. 4 shows the AFM images of surfaces of Pt electrodes, which in general were consistent with observations in top-view SEM images.

Fig. 5 shows the cyclic voltammograms from CV measurements for the GLAD Pt counter electrodes deposited at different substrate tilt angles. In these cyclic voltammograms, the cathodic current peaks (I_{PC}) between −0.55 V and −0.65 V correspond to the reduction of I_3^- ions through interaction with the Pt electrode. Thus, in general, the magnitude of the I_{PC} represents the catalytic capability (activity) of a counter electrode toward reduction of I_3^- in DSSCs. As seen in Fig. 5 and Table 2, the cathodic current peaks (I_{PC}) of the Pt electrodes Pt0°(200), Pt70°(200), Pt75°(200) and Pt85°(200) are 2.02 mA/cm^2, 2.41 mA/

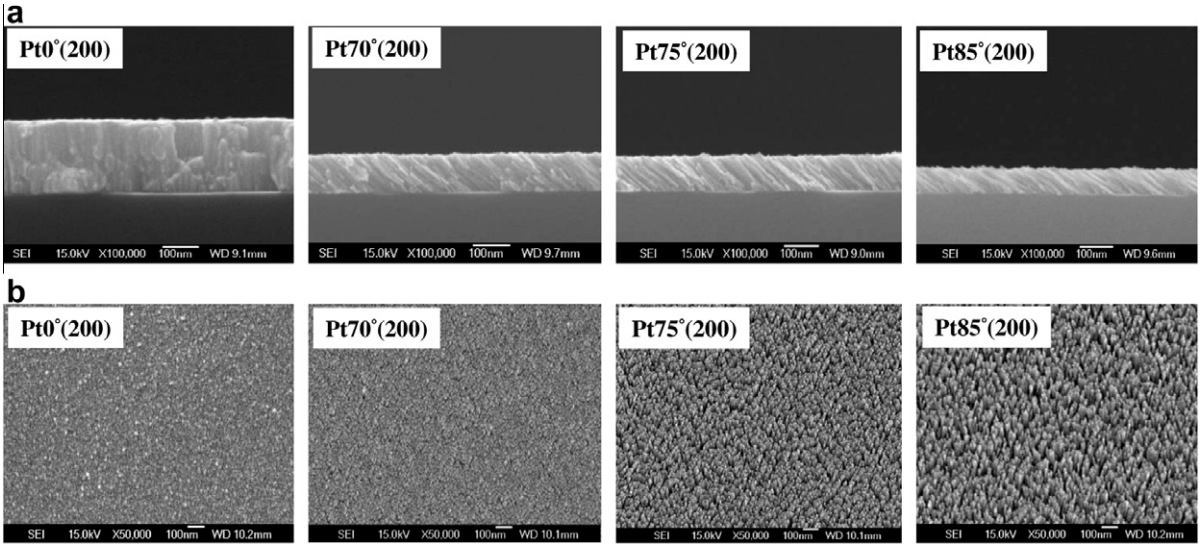

Fig. 3. (a) Cross-section and (b) top-view SEM images of Pt films deposited at different substrate tilt angles (set thickness = 200 nm).

Table 2
Characteristics of Pt electrodes deposited at different substrate tilt angles and set thicknesses.

Pt electrode	Substrate tilt angle α (°)	Set film thickness t_0 (nm)	Actual film thickness t_{actual} (nm)	Column tilt angle β (°)	Pt film roughness (nm)	CV I_{PC} (mA/cm^2)
Pt0°(200)	0	200	206.2	0	0.21	2.02
Pt70°(200)	70	200	100.3	42	0.87	2.41
Pt75°(200)	75	200	90.9	47	1.01	2.65
Pt85°(200)	85	200	74.1	56	1.71	2.24
Pt85°(300)	85	300	107.8	56	2.23	2.45

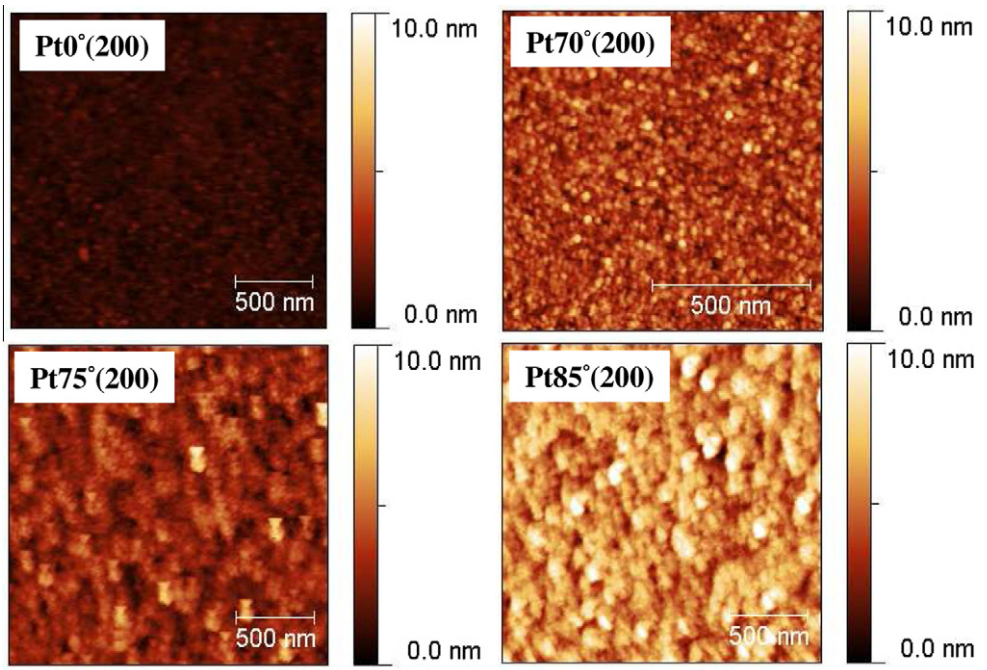

Fig. 4. AFM images of Pt films deposited at different substrate tilt angles (set thickness = 200 nm).

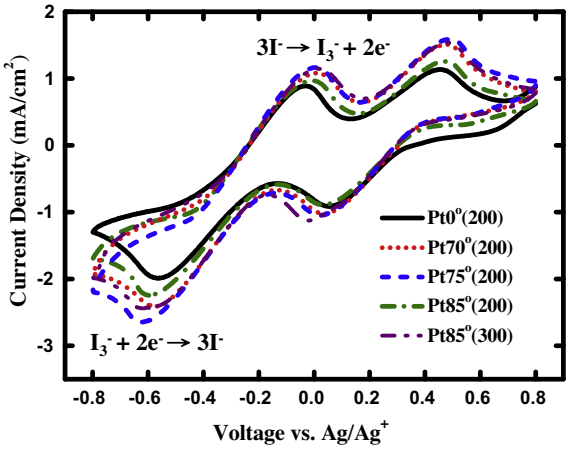

Fig. 5. Cyclic voltammograms of Pt counter electrodes deposited at different substrate tilt angles and set thicknesses.

cm^2, 2.65 mA/cm^2 and 2.24 mA/cm^2, respectively. The enhanced electro-catalytic activities of Pt electrodes Pt70°(200), Pt75°(200) and Pt85°(200) (vs. dense Pt electrode Pt0°(200)) are certainly associated with the increased active surface areas of GLAD Pt films [34]. These CV results clearly indicate that depositing Pt by the GLAD technique be an effective way to increase the active surface areas of the counter electrodes and thus to enhance their electro-catalytic ability (activity). Among the four Pt electrodes, Pt electrode Pt75°(200) gives the highest electro-catalytic ability. Pt electrode Pt85°(200) appears to have larger film porosity than Pt electrode Pt75°(200). Yet under the same material consumption (i.e., same set thickness t_0), the actual (vertical) thickness t_{actual} obtained for Pt electrode Pt85°(200) is significantly smaller than those for GLAD Pt electrodes Pt70°(200) and Pt75°(200). For a fair comparison, a GLAD Pt electrode Pt85°(300) with an actual layer thickness t_{actual} similar to that of Pt75°(200) was also prepared and tested (Table 2). The actual layer thickness t_{actual} of Pt electrode Pt85°(300) was estimated to be 107.8 nm. The cathodic current peak (I_{PC}) of the Pt electrodes Pt85°(300) is 2.45 mA/cm^2, which does increase with the Pt electrode thickness but is still lower than that of Pt75°(200). Although Pt85°(300) is already thicker than Pt75°(200), in Pt85°(300) the separation between inclined columns is larger and the column density is lower, and thus the electro-catalytic activity of Pt85°(300) is still lower than that of Pt75°(200). Thus in view of both material consumption and enhancement of electro-catalytic activity, there may be an optimal substrate tilt angle (e.g., $\alpha = 75°$) for GLAD Pt deposition, not the larger, the better.

3.2. Characteristics of DSSCs using nanoporous GLAD Pt counter electrodes

In this work, the FTO glass substrate FTO2% with a smaller roughness and optical haze (2%) was first used to study the influences of various nanoporous GLAD Pt counter electrodes (as listed in Table 2) on DSSC characteristics. After determining the effects of different GLAD Pt electrodes, the FTO glass substrate FTO17% with a larger texture and optical haze (17%) was then applied in combination with the picked GLAD Pt electrode to further optimize the DSSC performances.

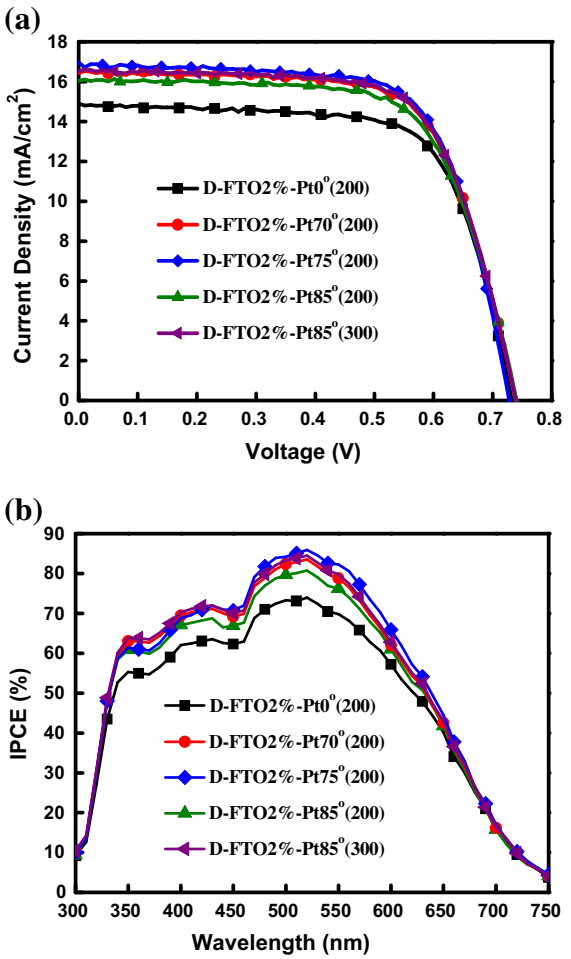

Fig. 6. (a) I–V, and (b) IPCE characteristics of DSSCs fabricated using the FTO glass substrate FTO2% and Pt counter electrodes deposited at different substrate tilt angles and set thicknesses.

Fig. 6(a) and (b) shows the I–V characteristics and IPCE characteristics, respectively, of the DSSCs fabricated on FTO glass substrate FTO2%, using various Pt counter electrodes. The photovoltaic characteristics of the five devices, including the short-circuit current (J_{SC}), the open-circuit voltage (V_{OC}), the fill factor (FF), and the conversion efficiency (Eff.), are summarized in Table 3. From Fig. 6(a) and Table 3, one sees that the open-circuit voltage (V_{OC}) and the fill factor (FF) do not differ among these five devices. Yet, compared to the device using the traditional normal-direction Pt deposition (device D-FTO2%-Pt0°(200)) with Pt electrode Pt0°(200), J_{SC} and power conversion efficiency of the devices using GLAD Pt electrodes are clearly enhanced. The J_{SC}, V_{OC} and FF of the DSSC based on Pt electrode Pt0°(200) are 14.91 mA/cm^2, 0.72 V and 0.69, respectively, yielding an overall conversion efficiency of 7.51%. Under the same conditions, the DSSCs based on GLAD Pt electrode Pt70°(200), Pt75°(200), Pt85°(200) and Pt85°(300) with enhanced electro-catalytic activities show enhanced J_{SC} and conversion efficiency of (16.44 mA/cm^2, 8.17%), (16.96 mA/cm^2, 8.47%), (16.04 mA/cm^2, 8.08%), and (16.52 mA/cm^2, 8.32%), respectively. The enhancements of the conversion efficiencies for DSSCs using GLAD Pt counter-electrodes Pt70°(200), Pt75°(200), Pt85°(200), and Pt85°(300) (vs. Pt0°(200)) are 8.78%, 12.78%, 7.59%, and 10.78%, respectively. The DSSC based on the Pt electrode Pt75°(200) ($\alpha = 75°$) shows the highest power conversion efficiency, consistent with electrochemical results from cyclic voltammetry.

The IPCE results of the DSSCs are shown in Fig. 6(b), in which one sees that the IPCE in general increases with the electro-catalytic activity (as examined by CV) of the corresponding Pt counter electrode. The peak IPCE increases from 73.2% of the device on Pt electrode Pt0°(200) ($\alpha = 0°$), to 85.8% of the device on Pt electrode Pt75°(200) ($\alpha = 75°$). As a result, the short-circuit current J_{SC} (Fig. 6(a), Table 3) also shows a corresponding enhancement in devices. Overall, the IPCE, short-circuit current, and power conversion efficiency of the DSSCs were enhanced by using the nanoporous GLAD Pt counter electrodes.

Previous reports revealed that fabricating DSSCs on highly textured FTO transparent conductors with larger optical hazes could enhance scattering and trapping of the incident light in the devices and thus enhance the absorption and power conversion efficiencies of devices [35]. Thus, the FTO glass substrate FTO17% with a larger texture and optical haze (17%) was then applied in combination with the picked GLAD Pt electrode (Pt75°(200), with $\alpha = 75°$) to further optimize the DSSC characteristics and performances.

Fig. 7(a) and (b) shows the I–V characteristics and IPCE characteristics, respectively, of the DSSCs fabricated on FTO glass substrate FTO17%, using Pt counter electrodes Pt0°(200) and Pt75°(200) (corresponding to device D-FTO17%-Pt0°(200) and device D-FTO17%-Pt75°(200), respectively). The photovoltaic characteristics of these two devices are also summarized in Table 3. In comparing device D-FTO17%-Pt0°(200) with device D-FTO2%-Pt0°(200) (or

Table 3
Characteristics of DSSCs fabricated using different Pt counter electrodes and different FTO substrates.

Device	FTO substrate	Pt electrode	J_{SC} (mA/cm^2)	V_{OC} (V)	FF	Eff. (%)	Peak IPCE (%)	R_{Pt} (Ω)
D-FTO2%-Pt0°(200)		Pt0°(200)	14.91	0.72	0.69	7.51	73.2	16.85
D-FTO2%-Pt70°(200)		Pt70°(200)	16.44	0.72	0.69	8.17	83.5	5.85
D-FTO2%-Pt75°(200)	FTO2%	Pt75°(200)	16.96	0.72	0.69	8.47	85.8	4.99
D-FTO2%-Pt85°(200)		Pt85°(200)	16.04	0.73	0.69	8.08	80.7	6.20
D-FTO2%-Pt85°(300)		Pt85°(300)	16.52	0.73	0.69	8.32	83.9	5.42
D-FTO17%-Pt0°(200)	FTO17%	Pt0°(200)	17.63	0.77	0.70	9.52	87.4	15.48
D-FTO17%-Pt75°(200)		Pt75°(200)	18.71	0.79	0.72	10.71	93.2	4.93

similarly comparing device D-FTO17%-Pt75°(200) with device D-FTO2%-Pt75°(200)), one sees that the adoption of the highly textured FTO transparent conductor did significantly enhance the J_{SC}, V_{OC}, power conversion efficiency, and IPCE (Fig. 7 and Table 3). With adoption of highly textured FTO, the J_{SC}, power conversion efficiency and peak IPCE of DSSCs increased from (14.91 mA/cm^2, 7.51%, 73.2%) of device D-FTO2%-Pt0°(200) (on FTO with haze = 2%) to (17.63 mA/cm^2, 9.52%, 87.4%) of device D-FTO17%-Pt0°(200) (on FTO with haze = 17%). The DSSCs fabricated on highly textured FTO glass substrates FTO17% show larger V_{OC} than devices fabricated on less textured FTO substrates FTO2%. The cause for this V_{OC} increment is not clear yet and requires further studies. More importantly, by combining the highly textured FTO with the nanoporous GLAD Pt counter electrode (i.e., device D-FTO17%-Pt75°(200)), the J_{SC}, V_{OC}, power conversion efficiency and peak IPCE of DSSCs were further enhanced to (18.71 mA/cm^2, 0.79 V, 10.71%, 93.2%). These results indicate that the enhanced electrocatalytic activity of the nanoporous GLAD Pt counter electrodes is generally beneficial to DSSC efficiency.

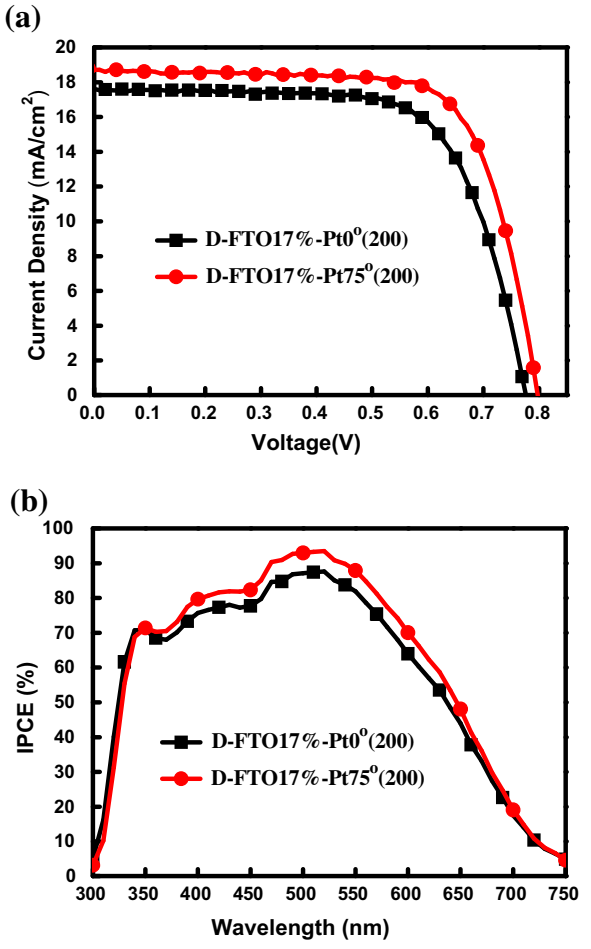

Fig. 7. (a) I–V, and (b) IPCE characteristics of DSSCs fabricated using the FTO glass substrate FTO17% and Pt counter electrodes deposited at substrate tilt angles of 0° (Pt electrode Pt0°(200)) and 75° (Pt electrode Pt75°(200)).

3.3. Electrochemical impedance spectroscopy of devices

The effects of GLAD Pt counter electrodes on photovoltaic characteristics of DSSCs were further investigated by electrochemical impedance spectroscopy (EIS). EIS is a useful tool for characterizing interfacial charge-transfer processes in DSSCs, such as the charge recombination at the TiO_2/dye/electrolyte interface, electron transport in the TiO_2 electrode, electron transfer at the counter electrode, and ion transport in the electrolyte [36]. In this study, EIS was conducted by subjecting the cell to the constant AM 1.5G 100 mW/cm^2 illumination and to the bias at the open-circuit voltage V_{OC} of the cell (namely, the condition of no DC current).

Fig. 8 shows the EIS Nyquist plots (i.e., minus imaginary part of the impedance $-Z''$ vs. the real part of the impedance Z' when sweeping the frequency) for device using various Pt counter electrodes. In the frequency range investigated (20 Hz–1 MHz), a larger semicircle occurs in the lower frequency range (~20 Hz–1 kHz) and a smaller semicircle occurs in the higher frequency range. The larger semicircles in the lower frequency range (~20 Hz to 1 kHz) are not complete due to the limited frequency range of our instrument (the lowest frequency is not low enough). With the bias illumination and voltage applied, the larger semicircle at lower frequencies corresponds to the charge transfer processes at the TiO_2/dye/electrolyte interface [37], while the smaller semicircle at higher frequencies corresponds to the charge transfer processes at the Pt/electrolyte interface [38]. The smaller semicircles corresponding to the Pt electrode show a significant difference between devices. It indicates that the impedance at the Pt/electrolyte interface was affected by different Pt counter electrodes.

By fitting the measured impedance characteristics of Fig. 8 with equivalent circuits of DSSCs [39], the charge-transfer resistances R_{Pt} (for the Pt/electrolyte interface) for devices fabricated using various Pt electrodes can be extracted and are summarized in Table 3. In general, the trend of the magnitude of R_{Pt} (vs. different Pt electrodes) is

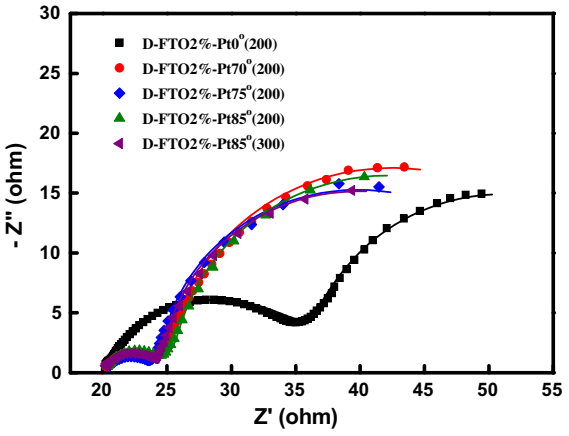

Fig. 8. Measured (symbols) and fitted (lines) EIS Nyquist plots for device fabricated using the FTO glass substrate FTO2% and Pt counter electrodes deposited at different substrate tilt angles and set thicknesses.

consistent with the electro-catalytic activity detected by cyclic voltammetry. Device D-FTO2%-Pt0°(200) with a dense Pt counter electrode shows a highest R_{Pt} of 16.85 Ω, while all devices with nanoporous GLAD Pt counter electrodes show significantly reduced R_{Pt} of 6.2 to 4.99 Ω. Among different GLAD Pt counter electrodes, Pt electrode Pt75°(200) ($\alpha = 75°$) gives the smallest R_{Pt} of 4.99 Ω, owing to its largest electro-catalytic activity. The decrease of R_{Pt} is correlated with the increase of the DSSC efficiency, indicating the ability of catalyzing the reduction of the I_3^- ions at the Pt/electrolyte interface and thus more efficient charge exchange at the Pt/electrolyte interface are enhanced with larger surface areas and electro-catalytic activity [40]. Overall, the EIS results are in good agreement with CV characteristics of various Pt electrodes and photovoltaic characteristics of various devices.

4. Conclusions

In conclusion, we report an effective way to produce nanoporous Pt counter electrodes of dye-sensitized solar cells by the glancing-angle deposition (GLAD) technique. By controlling the orientation of the substrate relative to the incident Pt vapor flux during the deposition, nanoporous films composed of inclined nm-scale columns were produced through the self-shadowing effect. Pt counter electrodes having varied nanoporous structures were characterized for their morphological and electrochemical properties, and were subjected to device studies to establish the correlation with DSSC characteristics/performances. The results suggest that the nanoporous GLAD Pt electrodes can effectively enhance active surface areas, the catalytic ability and charge exchange at the Pt/electrolyte interface of a DSSC. As a result, the quantum efficiency, short-circuit current, and power conversion efficiency of the DSSC can be enhanced by up to 12–13% with using the nanoporous GLAD Pt counter electrodes.

Acknowledgements

The authors gratefully acknowledge the financial support from AU Optronics Corporation, National Science Council (Grant NSC-99-2221-E-002-118-MY3), and Ministry of Education of Taiwan (Grant 10R70607-2).

References

[1] T. Bessho, S.M. Zakeeruddin, C.Y. Yeh, E.W.G. Diau, M. Grätzel, Angew. Chem. Int. Ed. 49 (2010) 6646.
[2] K.O. Ott, Prog. Nucl. Energy 29 (1995) 81.
[3] L.L. Kazmerski, Renewable Sustainable Energy Rev. 1 (1997) 71.
[4] B. O'Regan, M. Grätzel, Nature 353 (1991) 737.
[5] J. Jiu, S. Isoda, F. Wang, M. Adachi, J. Phys. Chem. B 110 (2006) 2087.
[6] A. Hagfeldt, M. Grätzel, Acc. Chem. Res. 33 (2000) 269.
[7] Y. Chiba, A. Islam, Y. Watanabe, R. Komiya, N. Koide, L. Han, Jpn. J. Appl. Phys. 25 (2006) 638.
[8] C.Y. Chen, M. Wang, J.Y. Li, N. Pootrakulchote, L. Alibabaei, C. Ngoc-le, J. Decoppet, J. Tsai, C. Grätzel, C.G. Wu, S.M. Zakeeruddin, M. Grätzel, ACS Nano 3 (2009) 3103.
[9] M. Grätzel, Nature 414 (2001) 338.
[10] A. Hauch, A. Georg, Electrochim. Acta 46 (2001) 3457.
[11] M. Wang, Y. Lin, X. Zhou, X. Xiao, L. Yang, S. Feng, X. Li, Mater. Chem. Phys. 107 (2008) 61.
[12] N. Papageorgiou, W.F. Maier, M. Grätzel, J. Electrochem. Soc. 144 (1997) 876.
[13] X. Fang, T. Ma, G. Guan, M. Akiyama, T. Kida, E. Abe, J. Electroanal. Chem. 570 (2004) 257.
[14] K. Suzuki, M. Yamagauchi, M. Kumagai, S. Yanagida, Chem. Lett. 32 (2003) 28.
[15] Z. Huang, X. Liu, K. Li, D. Li, Y. Luo, H. Li, W. Song, L. Chen, Q. Meng, Electrochem. Commun. 9 (2007) 596.
[16] Y. Saito, T. Kitamura, Y. Wada, S. Yanagida, Chem. Lett. 31 (2002) 1060.
[17] Y. Saito, W. Kubo, T. Kitamura, Y. Wada, S. Yanagida, J. Photochem. Photobiol. A 164 (2004) 153.
[18] Q.W. Jiang, G.R. Li, X.P. Xiao, Chem. Commun. 41 (2009) 6720.
[19] M. Wang, A.M. Anghel, B. Marsan, N.C. Ha, N. Pootrakulchote, S.M. Zakeeruddin, M. Grätzel, J. Am. Chem. Soc. 131 (2009) 15976.
[20] K. Robbie, M.J. Brett, A. Lakhtakia, Nature 384 (1996) 616.
[21] B. Dick, M.J. Brett, T. Smy, J. Vac. Sci. Technol. B 21 (2003) 23.
[22] M. Malac, R.F. Egerton, J. Vac. Sci. Technol. A 19 (2001) 158.
[23] C.M. Zhou, D. Gall, Thin Solid Films 516 (2007) 433.
[24] B. Dick, M.J. Brett, T. Smy, M. Belov, M.R. Freeman, J. Vac. Sci. Technol. B 19 (2001) 1813.
[25] L. Andrade, S.M. Zakeeruddin, M.K. Nazeeruddin, H.A. Ribeiro, A. Mendes, M. Grätzel, ChemPhysChem 10 (2009) 1117.
[26] M.K. Nazeeruddin, F.D. Angelis, S. Fantacci, An. Selloni, G. Viscardi, P. Liska, S. Ito, B. Takeru, M. Grätzel, J. Am. Chem. Soc. 127 (2005) 16835.
[27] S. Ito, N.L.C. Ha, G. Rothenberger, P. Liska, P. Comte, S.M. Zakeeruddin, P. Pechy, M.K. Nazeeruddin, M. Grätzel, Chem. Commum. (2006) 4004.
[28] H.W. Lin, S.Y. Ku, H.C. Su, C.W. Huang, Y.T. Lin, K.T. Wong, C.C. Wu, Adv. Mater. 17 (2005) 2489.
[29] R. Eichberger, F. Willig, Chem. Phys. 141 (1990) 159.
[30] C.J. Yang, T.Y. Cho, C.L. Lin, C.C. Wu, J. Soc. Inf. Disp. 16 (2008) 691.
[31] M. Grätzel, Photovoltaics Res. Appl. 8 (2000) 171.
[32] N. Vlachopoulos, P. Liska, J. Augustynski, M. Grätzel, J. Am. Chem. Soc. 110 (1988) 1216.
[33] K. Robbie, M.J. Brett, J. Vac. Sci. Technol. A 15 (1997) 1460.
[34] K.C. Huang, Y.C. Wang, R.X. Dong, W.C. Tsai, K.W. Tsai, C.C. Wang, Y.H. Chen, R. Vittal, J.J. Lin, K.C. Ho, J. Mater. Chem. 20 (2010) 4067.
[35] C.H. Tsai, S.Y. Hsu, T.W. Huang, Y.T. Tsai, Y.F. Chen, Y.H. Jhang, L. Hsieh, C.C. Wu, Y.S. Chen, C.W. Chen, C.C. Li, Org. Electron. 12 (2011) 2003.
[36] M. Adachi, M. Sakamoto, J. Jiu, Y. Ogata, S. Isoda, J. Phys. Chem. B 110 (2006) 13872.
[37] C.C. Chen, B.C. Huang, M.S. Lin, Y.J. Lu, T.Y. Cho, C.H. Chang, K.C. Tien, S.H. Liu, T.H. Ke, C.C. Wu, Org. Electron. 11 (2010) 1901.
[38] L.Y. Lin, C.H. Tsai, T.W. Huang, L. Hsieh, S.H. Liu, H.W. Lin, K.T. Wong, C.C. Wu, S.H. Chou, S.H. Chen, A.I. Tsai, J. Org. Chem. 75 (2010) 4778.
[39] Q. Wang, J. Moser, M. Grätzel, J. Phys. Chem. B 109 (2005) 14945.
[40] L.M. Peter, N.W. Duffy, R.L. Wang, K.G.U. Wijayantha, J. Electroanal. Chem. 524 (2002) 127.